Fuel 182 (2016) 340–351

Contents lists available at ScienceDirect

Fuel

journal homepage: www.elsevier.com/locate/fuel

Full Length Article

Physical model based reliability analysis for accelerated life testing of a fuel supply system

Elmar Pohl *, Roy T.E. Hermanns

OWI – Oel-Waerme-Institut GmbH, Affiliated Institute of the RWTH Aachen University, Kaiserstraße 100, 52134 Herzogenrath, Germany

HIGHLIGHTS

- A simulation approach for physical model based reliability analysis is introduced.
- A fuel supply system of a household oil burner is analyzed as a test case.
- The fuel supply system is modeled inclusive component and fuel degradation.
- A functional relation of stress factor and acceleration factor is described.

GRAPHICAL ABSTRACT

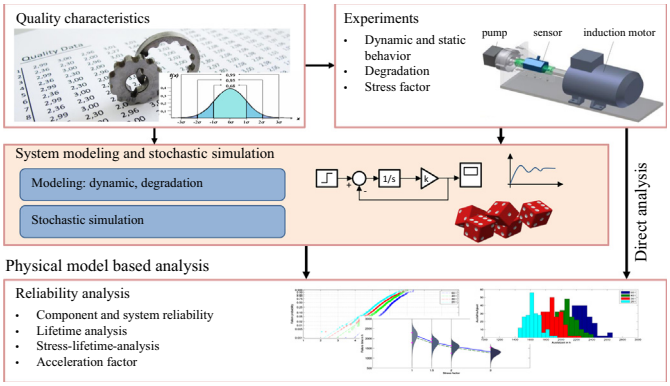

ARTICLE INFO

Article history:
Received 6 November 2015
Received in revised form 23 May 2016
Accepted 25 May 2016

Keywords:
Accelerated life testing
Stochastic simulation
Fuel supply system
Stress factor
Acceleration factor
Degradation modeling

ABSTRACT

In a fuel supply system of a conventional household oil heating system the fuel degrades over time depending on the system temperature, the tank volume and the flow rates. The test fuel is a blend of 80 vol.% conventional domestic heating oil and 20 vol.% fatty acid methyl ester from rapeseed oil feedstock. The fuel will increase the deposits in the fuel supply which lead to system failures. In this paper a model based approach is introduced for the analysis of accelerated life testings. The impact of the tank volume on the failure time is analyzed. A well balanced physical model is set up for stochastic simulation. The model contains short term dynamic and long term transient degradation effects that have an important impact on the system reliability. The degradation effects of the components and the used fuel cause a system failure over time. A system failure is detected when the volume flow of the fuel supply declines. The analysis shows that the typical variances of characteristic parameters lead to a significant distribution of failure time. Furthermore, the functional relation between tank volume as stress factor and failure time is described.

1. Introduction

A major problem of the reliability analysis of experimental data is that a large number of tests is needed in order to describe the statistical relations of component characteristics and failure time. With a low number of experimental samples a statistical analysis is difficult to achieve. Consequently the analysis is reduced to general statements and a complete statistical analysis of failure data is not possible. Commonly, due to cost and time reduction, only a part of a system can be analyzed in detail. Models for lifetime analysis are generally either data-driven or derived from physical principles via stochastic processes [1]. However, only a few methods

* Corresponding author.
E-mail address: e.pohl@owi-aachen.de (E. Pohl).

http://dx.doi.org/10.1016/j.fuel.2016.05.119
0016-2361/

Nomenclature

Roman letters

A	surface area
AF	acceleration factor
C	capacity
Da	Damköhler number
d	deflection distance
i	current
J	mass inertia
k	constant
L	inductance
M	torque
m	mass
$\dot{m}$	mass flow
n	rotation speed
p	pressure
$\dot{Q}$	thermal power
R	resistance
s	stress factor
t	time
U	voltage
$\dot{V}$	volumetric flow
V	volume
v	velocity

Greek letters

α	heat transfer coefficient
β	shape parameter
γ	location parameter
ϵ	motor specific constant
Φ	source term
ϕ	dynamic viscosity
ψ	motor specific constant
ρ	density
θ	temperature
τ	residence time
ζ	pressure loss coefficient
μ	mean
σ	standard deviation
ω	angle speed

Indices

a	accelerated
Byp	bypass
Cap	capacitor
F	filter
fl	fluid
K	cake
lam	laminar
$MTTF$	mean time to failure
Mot	motor
Noz	nozzle
n	non-accelerated
O	orifice
oxi	oxidation
P	Piston
Pre	preheater
PRV	pressure relief valve
r	rotor
s	stator
th	theoretical
tur	turbulent

have been introduced so far to support Model Based System Engineering (MBSE) and Reliability, Availability, Maintainability, Safety (RAMS) activities e.g. MeDISIS [2], SysML models [3], RAMSAS [4,5] or physical models maintenance modeling [6]. The reason is mainly due to absence of a consistent modeling framework including physical models and degradation effects. A major benefit of a physical modeling approach, however, is that the simulation of validated models can be repeated under different boundary conditions.

1.1. Principles for accelerated life testing modeling

Accelerated tests are distinguished on the observed property. While accelerated life testing (ALT) generate information on failure time, the accelerated degradation test (ADT) is used for the explicit temporal description of degradation data [7]. Most of the underlying principles are the same for both ALT and ADT. ADT modeling is commonly performed using regression models for the description of degradation paths. In this paper physical models describe the aging behavior, hence, in the following the more general principles of ALT are introduced. ALT is a standard technique in industry to reduce the test time of products and has created numerous literature and industry standards [8–15]. However, most of the approaches use statistical analysis of experimental data only, without considering physical background using models. A good overview on data-driven regression models are found in the works of Lu, Meeker, Escobar and others e.g. [16–19]. A generic design of an ALT program is summarized by Escobar and Meeker [19].

- The ALT related to an *increased use rate* is performed by increasing load cycles per time. An example of this approach is described in Dowling [20]. In this work, the crack growth of metals has been described as a function of the load cycles.
- In ALT related to *increased environmental influences*, the degradation is accelerated by chemical or physical mechanism. Examples are found in the degradation of fuels by UV radiation [21].
- In ALT with *increased aging rate* temperature and humidity are changed in such a way that chemical processes lead to certain failure mechanisms. For the temperature-dependent aging behavior of liquids and gases the Arrhenius approach and Eyring approach is chosen. Liška [21] used the Arrhenius approach for the description of the aging behavior of fuels.
- In ALT related to *increased stress*, degradation will be caused by increased tension, pressure, voltage or other process variables.

The ALT models contain an *acceleration factor*, that is defined as the relation of accelerated and non-accelerated failure time [19]. The *stress factor* is a characteristic change in the system operation in order to force the degradation behavior. It is commonly defined as the relation of two physical values (e.g. load cycles, temperatures, etc.). The choice of a suitable stress factor is determined by the materials and the operation of the technical system. In ALT, methods are used to specify the effects of stress factors on the system behavior. In general, one or multiple stress factors can be used simultaneously [22]. Besides the standard approach different variants exist. When the stress factor is gradually increased with time, the test is called a step-stress accelerated life testing (SALT). The

progressive accelerated life testing (PALT) is a method with continuously increased stress factor.

1.2. Aging behavior of fuels

The fuel stability is in general the resistance of a fuel to degradation processes that can change fuel properties. Dunn [23] describes the principle mechanism for fuel degradation:

- Oxidation or autoxidation from contact with oxygen present in ambient air;
- thermal or thermal-oxidative decomposition from excess heat;
- hydrolysis from contact with water or moisture in tanks and fuel lines; or
- microbial contamination from migration of dust particles or water droplets containing bacteria or fungi into the fuel.

When bio fuel is oxidized, the resulting sediments can negatively influence the performance of the fuel system [24]. Liška [21] showed, that the failure time of components correlate with the oxidation stability of fuels. The models for oxidation stability based on experimental data have been documented by various authors, e.g. [25–27], using an Arrhenius approach for the temperature dependent aging of fuels. This approach will be used for the description of bio fuel aging and component failure analysis in this work.

1.3. Scope and outline of this paper

Classical reliability analysis of ALT rely on empirical statistical relations without the inclusion of physical models. In this work we present a novel approach combining physical models and stochastic simulation with classical methods of reliability analysis. Fig. 1 summarizes the approach used in this paper. Starting with quality characteristics, the variances of model parameters are used as boundary conditions for the system modeling and stochastic simulation block. The system modeling and stochastic simulation consists of a modeling step including dynamic short term and transient long term behavior. A novel simulation approach is set up without using a superordinate framework. Classical methods, among them reliability analysis and stress-lifetime analysis, are performed on the simulated failure time. As a test case the reliability of a fuel supply system using a blend of 80 vol.% conventional domestic heating oil and 20 vol.% fatty acid methyl ester from rapeseed oil feedstock is analyzed here. Three different objectives are considered in this paper:

1. Introduction of a consistent simulation approach for ALT using physical models,
2. analysis of the expected distribution of failure time,
3. proof of test design and functional description of stress factor and acceleration factor.

The paper is structured as follows. In the second section a formal methodology for the description of a stochastic simulation of degradation models is introduced. In the third section the test case of a fuel supply system is presented including the experimental observations and model validation. In the fourth section the reliability analysis is performed. Finally the conclusions and discussion are presented.

2. Methodology: stochastic simulation of degradation effects with physical models

The stochastic simulation approach presented in this work is explained in three steps. In a first step the modeling principles for lifetime analysis are introduced. This step includes the requirements for the numerical modeling approach. In a second step, the formal structure of the simulation procedure is introduced. After the stochastic simulation of system failure behavior, the failure data are analyzed with classical statistical approaches and a functional expression of failure time depending on the stress factor is presented in a third step.

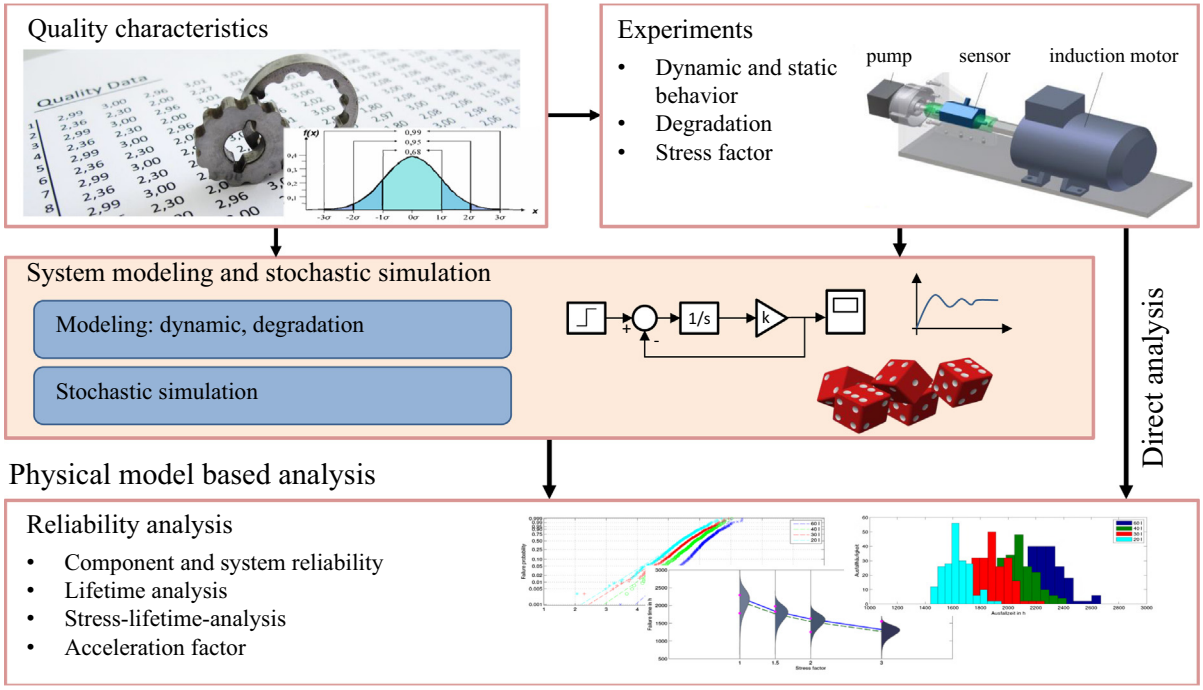

Fig. 1. Overview on the analyses and simulation approach.

2.1. Modeling principles for lifetime analysis

The simulation approach presented here uses physical models that are commonly applied in product development. The governing equations, e.g. energy and mass balances, are formulated as differential equations considering the dynamic short term behavior. The most important issue is the inclusion of the degradation behavior, which is called long term behavior.

2.2. Algorithm

The simulation algorithm consists of initialization of the model parameters, the simulation loops and the statistical analysis of the failure data. The sequence of the stochastic simulation is summarized in the structogram in Fig. 2. In a first step, the initialization of the model parameters is performed, while two different kind of parameters have to be distinguished. The *constant* model parameters do not change over the simulation runs (e.g. physical constants). The *random samples* represent quality differences (e.g. geometrical tolerances) related to each simulated system. The nature of the random parameter sets can be freely defined, e.g. modeled statistically dependent or independent. In a second step, the stochastic simulation is performed in three loops. The outer loop (A) is passed for each stress factor *s*. The stress factors are imposed to the system operation in order to analyze the failure behavior. The middle loop (B) runs for each group of samples *N* and terminates when a defined maximum simulation sample N_{max} is completed. In the inner loop (C) *M* simulation blocks are simulated in parallel. Since the inner loop can be simulated in parallel, the simulation is much faster than a sequential simulation.

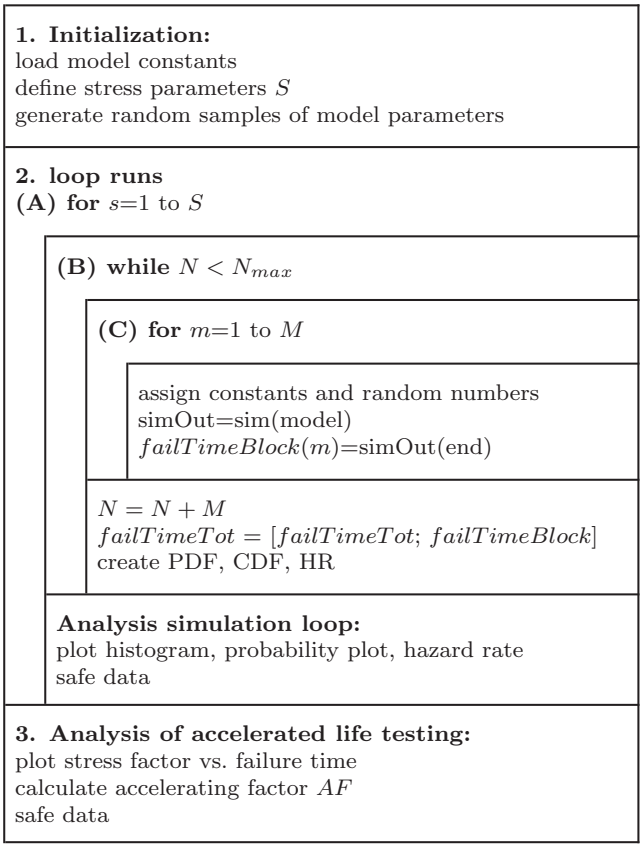

Fig. 2. Structogram for the stochastic simulation approach.

2.3. Analysis

In a third step, the lifetime analysis is carried out. The failure time is determined using a fault detection method with limit checking or any other fault detection method [28]. The parameters for the distribution function are fitted with the simulated failure data. With the resulting parameters the probability density function (PDF), the cumulative distribution function (CDF), the hazard rate and histograms are determined. In the following test case, an experimental set of observations has been made with failure free time. Hence, the commonly used three parameter Weibull distribution is proposed and discussed in reliability analysis.

The general cumulative distribution function of the three parameter Weibull distribution is

$$F(t) = 1 - \exp\left[-\left(\frac{t-\gamma}{\eta}\right)^{\beta}\right], \tag{1}$$

with η as scale parameter, β as shape parameter, γ as location parameter (or failure free life) and t as the operating time. The simplest acceleration model assumes a linear effect over time. Therefore, the acceleration factor *AF* is introduced as

$$AF = t_n/t_a, \tag{2}$$

with t_n as the failure time under non-accelerated condition (index n) and t_a the failure time under accelerated condition (index a). Assuming a linear ALT model the acceleration factor is also the relation of the non-accelerated and accelerated scale parameter and location parameter [29]

$$AF = \eta_n/\eta_a = \gamma_n/\gamma_a. \tag{3}$$

The relation between the failure probability under non-accelerated conditions F_n and accelerated conditions F_a can be expressed by combining Eqs. (1) and (2)

$$F_n(t_n) = F_a(t_a) = F_a\left(\frac{t_n}{AF}\right) = 1 - \exp\left[-\left(\frac{t_n/AF - \gamma_a}{\eta_a}\right)^{\beta}\right]$$
$$= 1 - \exp\left[-\left(\frac{t_n - \gamma_a AF}{\eta_a AF}\right)^{\beta}\right]. \tag{4}$$

The three parameters of the Weibull function are fitted to the numerical failure data using the least squares procedure. With the χ^2 test the distribution is checked with the simulated data. The functional relation between the stress factor *s* as a process variable and the acceleration factor *AF* as a statistical parameter of the distribution function will be demonstrated with a test case, including degradation of fuels in a domestic oil heating system.

3. Description of a fuel supply system

3.1. Experimental tests

Liška et al. [30] described the degradation behavior of the hydraulic–mechanical part of a fuel supply system of a domestic oil heating system caused by degrading bio fuels. The design of the experimental test rig is summarized in Fig. 3. The system consists of the hydraulic components and a tank. In real applications only a part of the fuel passes the nozzle for combustion. The remaining fuel is fed back to the tank. Hence, in order to enforce rapid degradation of the fuel supply system, the ALT experiment was carried out without combustion. Since the fuel is pumped around in a loop, the tank volume has a significant impact on the system degradation. The tank volume is varied in multiple stages and lead to decreasing failure time with decreasing tank volume. The test rig was set up with following operating conditions [30]:

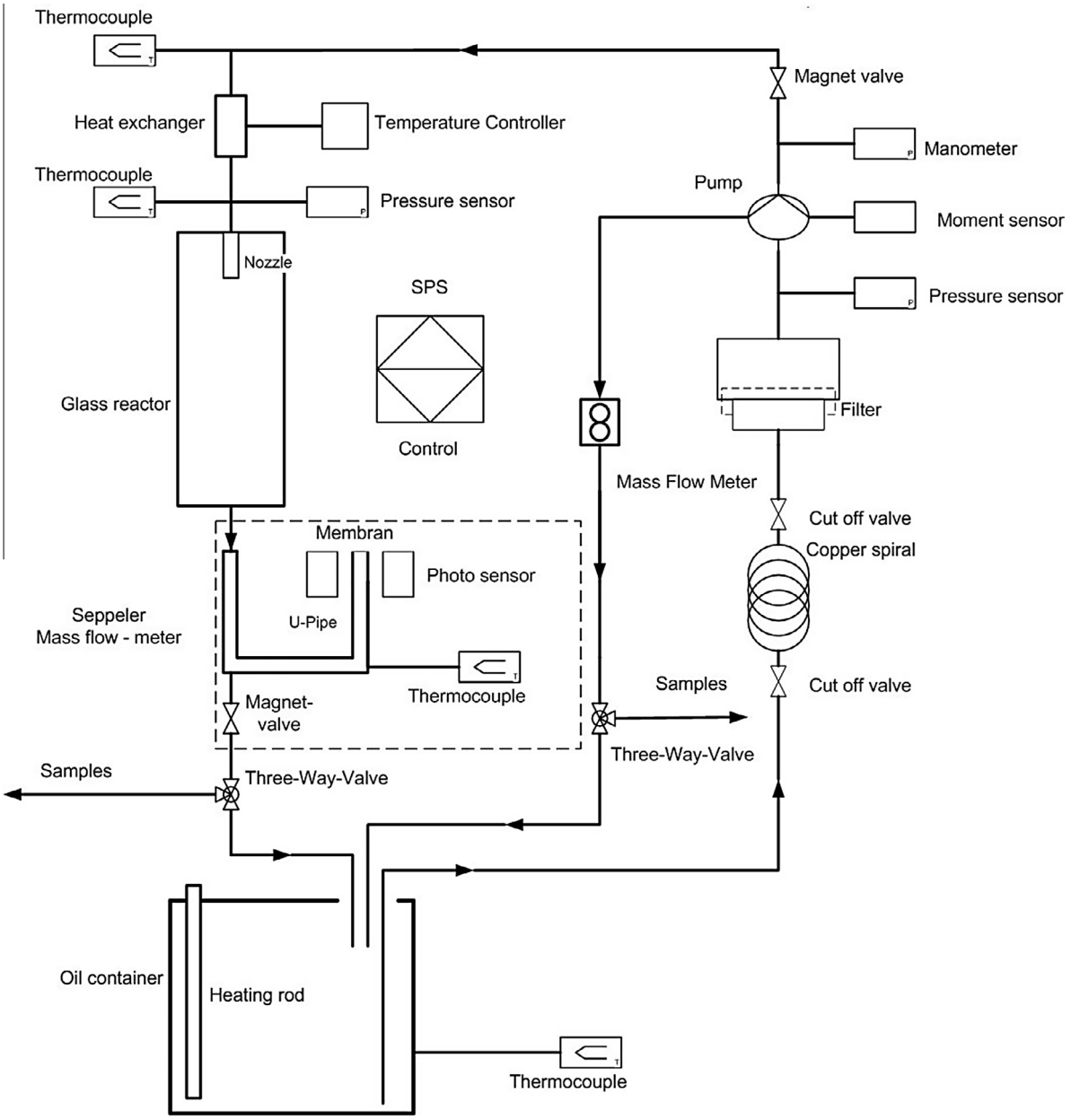

Fig. 3. Set up of the experimental test rig including components, measurement and control devices [30].

- Pump pressure 10 bar ($\dot{V}_{Noz} \approx 1.2\,\mathrm{l\,h^{-1}}$),
- temperature after preheater $\theta_{Pre} = 75\,^{\circ}\mathrm{C}$,
- temperature in tank $\theta_{Tank} = 35\,^{\circ}\mathrm{C}$,
- intermittent operation: 45 h of continuous operation, 3 h break,
- length of copper spiral 12 m,
- max. operating time 4000 h,
- tank volume $V_{Tank} = 60$, 40, 30 and 20 l.

In the experiment, eight identical systems were investigated in parallel. Two systems each were operated with the same tank volume. System number 1 and 5 were operated with 60 l, 2 and 6 with 40 l, 3 and 7 with 30 l and 4 and 8 with 20 l tank volume respectively. The experiments are grouped in sets with index i as summarized in Table 2. The test fuel is a mixture of domestic heating oil (DHO) and 20 vol.% fatty acid methyl ester (FAME). The DHO has specifications according to DIN 51603-1 and contains no performance additives. The FAME meets the requirements of EN 14214.

In the fuel tank, the fuel is stored and pre-conditioned to a temperature of $\theta_{Tank} = 35\,^{\circ}\mathrm{C}$. The temperature of the tank is conditioned by an electric heater. The fuel passes a copper spiral and enters the pre-filter. The pump is constructed as a two-pipe system. The pressureless return pipe of the pump is fed directly back into the tank. The pressurized volume flow is led through a valve to the preheater. The preheater conditions the fuel temperature to $\theta_{Pre} = 75\,^{\circ}\mathrm{C}$. Behind the nozzle the fuel is released to ambient pressure. The aerosol is liquefied in a glass cylinder and returns back into the tank. The overview of the setup presented in Fig. 3 also shows the installed measurement devices for temperature, pressure and volume flow.

Fig. 4 summarizes the failure times for each experimental system of the components preheater, nozzle and pump, measured by Liška et al. [30]. After a component failure, the component is changed and the experiment continues. In general the order of failures started with the nozzle, the preheater and finally the pump.

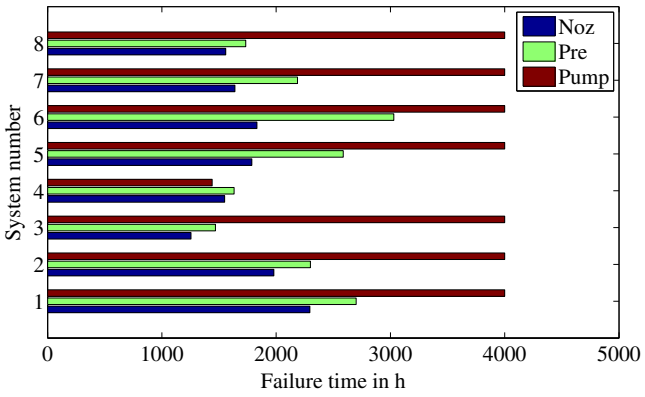

Fig. 4. Failure time of the system components [30].

However, the order of failure does not always correlate with the tank volume. In order to analyze the reliability of the system, a numerical simulation is performed with a validated system model of the experimental set up.

Beside the long term tests, several characterization tests of the components has been performed in order to obtain the quality characteristics. The results are used as the input parameters of the stochastic simulation and are tabulated in Appendix A.

3.2. Fuel aging

For the description of a temperature dependent aging behavior of the fuel, the Arrhenius equation is used. Various authors have determined the temperature dependence of the fuel aging based on oxidation stability. The reaction rate constant of the oxidation k_{oxi} is described with

$$k_{oxi} = A \cdot \exp(-E_A/R\theta), \tag{5}$$

where A is the pre-exponential factor in h^{-1}, E_A is the activation energy in $J\,mol^{-1}$, R is the universal gas constant in $J\,mol^{-1}\,K^{-1}$ and θ is the temperature in K. The coefficients for the Arrhenius equation used in this experimental set up according to Liška [21] are summarized in Table 1. The given data for the Arrhenius equation describe the temperature dependent aging behavior of the fuel. This Arrhenius approach describes that the reaction rate constant increases with increasing temperature. Hence, the preheater causes the highest thermal stress, since this is the location with the highest temperature in the system. However, only a minor part of fuel is passed through the preheater and nozzle. These contrary effects on degradation behavior are analyzed in detail in the description of the stress factor.

3.3. Description of the stress factor

The reduction of the tank volume reduced the failure time of the components, so that the reduction of the tank volume is an influencing factor in the ALT. In previous studies [21,30], it was shown that the fuel is aging with higher temperatures in particular. The resulting deposits from the aging products are responsible for the filter plugging of the preheater and the nozzle and other mechanical components that happen to be in contact with the fuel and may cause a system failure. Consequently, the temperature is considered as the second variable next to the tank volume. In the system shown in Fig. 3, there are two places where the temperature is regulated: in the preheater and the fuel tank. While the preheater keeps the fluid temperature at $\theta_{Pre} = 75\,^{\circ}C$, the temperature in the tank $\theta_{Tank} = 35\,^{\circ}C$ is significantly lower. According to the Arrhenius equation, the relative high temperature in the preheater leads to a faster fuel aging. However, the tank volume is significantly larger than the volume of the preheater so that a large part of the fuel is not exposed to the high temperature. About 10% of the volume flow is pumped through the preheater and the nozzle, the majority of the volume flow returns back to the tank through the bypass. The volume flow that experiences the temperature increase is thus relevant as the third variable.

Table 1
Aging characteristics of a bio fuel with 20% FAME [21].

Stability in h			Exp. factor in K^{-1}	Preexp. factor in h^{-1}
90 °C	110 °C	130 °C	E_A/R	A
58.0	13.0	3.1	10.706	$1 \cdot 10^{11}$

A dimensionless number that relates the variables volume, volume flow and temperature is the first order Damköhler number. The Damköhler number relates the reaction timescale (reaction rate constant) to the convection timescale (flow rate) for continuous or semibatch chemical processes [31]. First, the residence time τ is defined as the ratio of the volume and the volume flow in a reactor. Second, the temperature dependence is directly included in the reaction rate constant k_{oxi}. Hence, the dimensionless Damköhler number is now expressed with

$$Da_I = \tau k_{oxi} = (V/\dot{V})k_{oxi}. \tag{6}$$

With the Damköhler number one can now compare the influence of the preheater and the tank on the fuel aging. Fig. 5 shows the variation of the ratio $Da_{I,Pre}/Da_{I,Tank}$ as a function of the tank volume and the tank temperature. Up to a tank temperature of about 50 °C the ratio is greater than one, indicating that a significant proportion of the reaction products is caused by the preheater. However, from about 50 °C and higher tank temperature, the contribution of the tank is larger than the contribution of the preheater. This however, implies that a variation of the tank volume has no influence on the fuel-related failure time. When the ratio of Damköhler number is greater than one, a larger tank volume has a retarding effect on the fuel aging.

The reduction of the tank volume is also a reduction of residence time, since the volume flow of the pump remains constant over time. The stress factor s_i for each experimental set i is now defined with

$$s_i = \tau_1/\tau_i, \tag{7}$$

as a relative residence time. The dimensionless stress factor is related to the tank volume of 60 l, with $\tau_1 = 1.50$ h. The corresponding stress factor s_i for each experimental set i is summarized in Table 2. A tank volume of $V_{Tank} = 20$ l leads to a 3 times higher

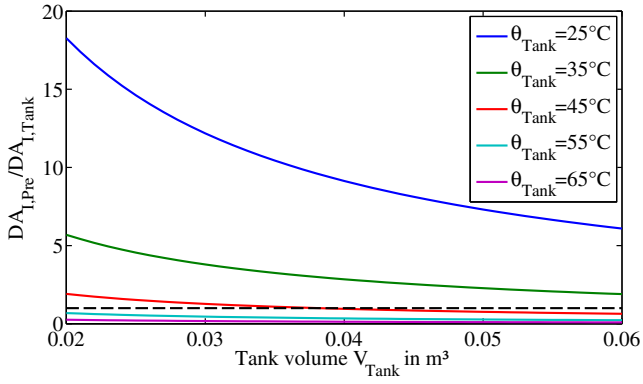

Fig. 5. Relation of the Damköhler number of the preheater $Da_{I,Pre}$ and the tank $Da_{I,Tank}$. The dashed line represents the case $Da_{I,Pre} = Da_{I,Tank}$.

Table 2
Relation between volume and stress factors of the system.

i	1	2	3	4	–
V_{Tank}	60	40	30	20	l
System no.	1, 5	2, 6	3, 7	4, 8	
τ_i	1.50	1.00	0.75	0.50	h
s_i	1.00	1.50	2.00	3.00	–

physical stress compared to the reference case at $V_{Tank} = 60$ l. This ALT is an increase of use rate as described in the introduction.

3.4. Physical model

In order to perform the reliability analysis of the system a physical model is set up and validated with the experimental data. The complete physical models consists of the models for the *mechanical components* (components that lead to system failure according to Fig. 4: induction motor, fuel pump, preheater and nozzle) and the *fuel*. All the models of the components can cause a failure of the complete system, hence the system characteristics and degradation behavior of each component has to be analyzed. The physical model consists of the dynamic system models and the degradation models. The dynamic system models are explained in Appendix A. The degradation models are described briefly.

Components. The induction motor can fail through very different failure modes. During experimental observation of this component a degradation of the capacitor could be identified. The decreasing capacity of the capacitor leads to decreasing starting torque of the motor. The degradation behavior of capacitors has been described by various authors, e.g. Kulkarni et al. [32]. The degradation of the induction motor is described by

$$\frac{dC_{Cap}}{dt} = -k_{Cap}, \tag{8}$$

which represents a simple linear degradation behavior of the capacitor over time. The degradation rate k_{Cap} is the capacity loss per time. The start value of $C_{Cap,0} = 2.99$ µF is reduced by k_{Cap} times the operating time t.

The experimental observations have shown the formation of deposits on components with fuel contact. The deposits lead to pressure loss in the fuel system until the volume flow was insufficient and the system failed. For the description of the degradation behavior of the preheater, an extended Bernoulli equation is set up. The pressure loss of the preheater is

$$\Delta p_{Pre} = \zeta_{Pre}\, v_{fl}^2 \rho_{fl}/2, \tag{9}$$

with ζ_{Pre} as the pressure loss coefficient, v_{fl} as the fluid velocity and ρ_{fl} as the fluid density. The pressure loss coefficient increases over time and is dependent on the concentration of the degradation products of the fuel. The degradation of the pressure loss coefficient ζ_{Pre} is here described with

$$\frac{d\zeta_{Pre}}{dt} = k_{part,1}\dot{m}_{part}. \tag{10}$$

The start value $\zeta_{Pre,0}$ is a component specific loss that is present at the beginning of the observation time. It can be estimated by measuring the pressure drop of the preheater at the beginning of the test. It is assumed, that the deposits from fuel degradation lead to pressure losses over time. The deposits originate from aging products $\dot{m}_{part}$ of the fuel. The parameter $k_{part,1}$ is a proportional scaling factor and can be determined by measuring the increasing pressure drop of the preheater over time.

For the description of the system behavior and degradation behavior of the oil burner nozzle the Darcy equation is set up in combination with the equation for the orifice. The total pressure loss over the nozzle Δp_{Noz} is

$$\Delta p_{Noz} = \Delta p_O + \Delta p_F + \Delta p_K, \tag{11}$$

with Δp_O as the pressure loss of the orifice, Δp_F the pressure loss of the filter and Δp_K the pressure loss of the filter cake. The orifice equation is used for the description of the nozzle hole. The volume flow is proportional to the root of the pressure, hence

$$\Delta p_O = \frac{\rho_{fl}}{2}\left(\frac{\dot{V}_{Noz}}{A_O}\right)^2 = \frac{\rho_{fl}}{2A_O^2}\left(\frac{dV_{Noz}}{dt}\right)^2. \tag{12}$$

With the assumption that the height and permeability of the filter stays constant over time, the pressure loss of the filter is described by

$$\Delta p_F = \frac{h_F}{B_F}\phi_{fl}\frac{\dot{V}_{Noz}}{A_F} = b\phi_{fl}\frac{1}{A_F}\frac{dV_{Noz}}{dt}. \tag{13}$$

The constants for filter height h_F and permeability B_F are summarized in factor b. The filter cake growths over time due to deposition of fuel aging products. With the Darcy equation the resulting pressure loss for the filter cake is defined as

$$\Delta p_K = \frac{h_K}{B_K}\phi_{fl}\frac{\dot{V}_{Noz}}{A_F} = \frac{k_{Noz}}{B_K}\phi_{fl}\frac{V_{Noz}}{A_F^2}\frac{dV_{Noz}}{dt}. \tag{14}$$

The volume of the filter cake is assumed to be proportional to the passed volume V_{Noz}. Hence, a proportional factor $k_{Noz} = (h_K A_F)/V_{Noz}$ is introduced. With

$$\Delta p_{Noz} = \left(\frac{\rho_{fl}}{2A_O^2}\frac{dV_{Noz}}{dt} + \frac{\phi_{fl}}{A_F}\left(\frac{k_{Noz}}{B_K A_F}V_{Noz} + b\right)\right)\frac{dV_{Noz}}{dt} \tag{15}$$

a compact differential equation for the complete nozzle behavior including degradation is set up. The term $k_{Noz}/B_K A_F$ describes the degradation behavior of the nozzle filter. Since the deposits depend on the particle concentration in the pumped fluid, it is assumed that the parameters $k_{Noz}/B_K A_F$ are related to the actual particle flow. Hence,

$$\frac{k_{Noz}}{B_K A_F} = k_{part,2}\dot{m}_{part} \tag{16}$$

with $k_{part,2}$ as a proportional scaling factor. Similar to the preheater, the term describes the pressure drop over the nozzle that leads to reduced volume flow. The parameter $k_{part,2}$ can be estimated with the volume flow and pressure drop of the nozzle. With the model equations the degradation behavior can be analyzed.

The system pressure over the time is shown in Fig. 6. One can see that the pressure is increasing over the time with different increasing rates. The pressure increase originates from an increase

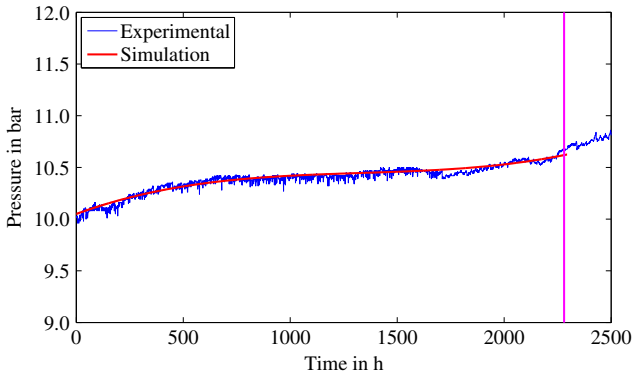

Fig. 6. Pressure of the nozzle over the time.

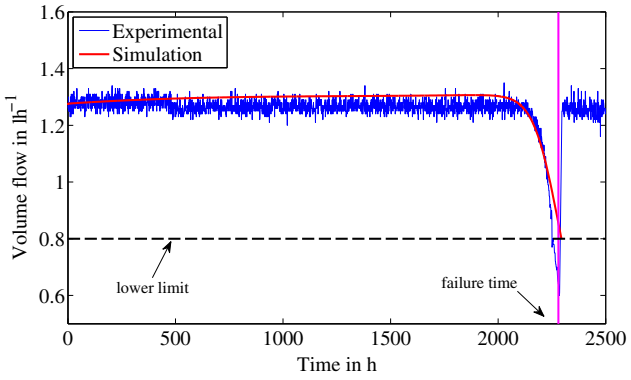

Fig. 7. Volume flow of the nozzle over the time.

in pump capacity over the time. Fig. 7 shows the corresponding volume flow of the experimental set up and the numerical model over time. A system failure is detected, when the volume flow is lower than $\dot{V}_{Noz} = 0.8\,\mathrm{l\,h^{-1}}$. This behavior is a crucial system information that describes the degradation path of the system. The physical model has been validated under different operating conditions, including the variation of tank volume and temperature.

Fuel. In the numerical model we assume that the fuels can create deposits that change the behavior of the system components. The temperature dependency of the fuel has already been introduced in Eq. (5). Following equation describes the mass balance for the fuel and a deposit (index *part*) that is created by oxidation.

$$\frac{dm_{fuel}}{dt} = \sum \dot{m}_{in,fuel} - \sum \dot{m}_{out,fuel} - \Phi \tag{17}$$

$$\frac{dm_{part}}{dt} = \sum \dot{m}_{in,part} - \sum \dot{m}_{out,part} + \Phi \tag{18}$$

The source term $\Phi = Vk_{oxi}/\rho_{fl}$ is the amount of fuel that is converted to oxidation products and is subtracted to the fuel balance and added to the balance of oxidation products. The creation of fuel aging products is connected to the component behavior.

4. Reliability analysis of the components and system

As described in the introduction, the present test is an ALT with increased use rate with s as one single stress factor. The goal of the present analysis is now to determine the impact of the quality characteristics of the physical model with respect to reliability. As shown in the experimental analysis, the system behavior changes over the time. The system output of one component is usually the input of another component. Hence, when the output is not constant over the time, the other component is also effected.

4.1. Failure modes of the components

Since the components suffer different failure modes, the main components motor-pump, preheater and nozzle are analyzed in detail.

Motor-pump-subsystem. The induction motor may fail caused by different failure modes. During operation, for example, a failure due to overloading of the motor windings can occur. During start-up it may happen that the starting torque of the engine is below the load torque of the pump. In this case, the system fails immediately, without starting the motor. The experiments have shown that the time scales for the failures caused by exceeding the starting torques occur much earlier than the failure due to mechanical wear or overloading. In the following analysis, therefore, only the comparison of the starting torque is performed.

The analysis of the induction motor is performed with the following assumptions:

- A failure of the motor is only possible when the motor-pump system is starting. Hence, no incipient (soft) failures occur,
- a failure is identified, when the starting torque of the motor is smaller than the torque of the pump.

Similar to the induction motor the pump fails due to several failure modes. The causes include exceeding a critical starting torque, the alleviation of the spring in the pressure relief valve or the mechanical wear of the gears and thus extremely high internal leakage. Numerical analysis and experimental observations have shown that an increase of leakage losses is barely visible for the other components preheaters and oil nozzle. The failure due to excessive leakage losses could not be observed on the test bench within the observed period. Because of deposits in the fuel pump an increase in the starting torque was observed on the test bench. In combination with the degradation of the induction motor (here the starting torque decrease due to the declining capacity of the capacitor), this behavior can lead to failures that may occur during the observation period. Since the assignment of the failure to induction motor or pump is not effective, the failure of the pump and induction motor are joint. A failure of the motor-pump unit occurs when the motor torque is smaller than the starting torque of the pump. The degradation of the capacitor now causes a decreasing starting torque of the motor over time, while the deposits in the pump cause an increasing starting torque of the pump.

Fig. 8 shows the histogram of the startup torque of the engine and the pump at the start $t = 0$ h of the experiment. The abscissa shows the torque in Nm and the ordinate represents the frequency of the simulated starting torques. In the illustrated stochastic simulation $n = 2000$ runs were performed. Due to the relative narrowness of the capacitor capacity of the motor, the variation of the engine torque is significantly smaller than that of the pump. The torques are relatively far apart so that no failure is expected.

Fig. 9 shows the distribution of simulated torques after 4000 h. Over time, the distributions are approaching which can lead to an overlap of the distribution functions. A definition of the failure probability $F = Pr(M_{Pump}(t) \geqslant M_{Mot}(t))$ is appropriate for the description of the motor-pump failure. This definition includes the failure criterion previously defined (failure due to reduced volume flow at the nozzle below $\dot{V}_{Noz} \leqslant 0.8\,\mathrm{l\,h^{-1}}$). With time, the starting torque becomes too low to accelerate the pump to nominal speed. As a consequence, the volume flow of the nozzle is not sufficient and leads to a failure. In simulation the aging of the motor-pump-subsystem could be observed, but did not lead to system failure, since other components failed before.

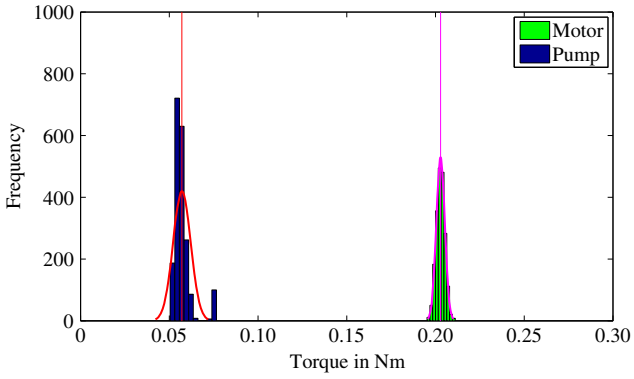

Fig. 8. Histogram of motor and pump starting torques with $n = 2000$ samples at $t = 0$ h.

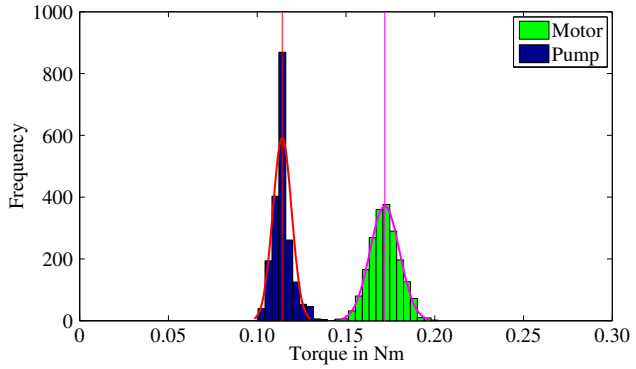

Fig. 9. Histogram of motor and pump starting torques with $n = 2000$ samples at $t = 4000$ h.

Preheater. The preheater consists of a heat exchanger, which can block due to deposits. The deposit in the preheater leads to a pressure drop so that the nozzle reduces the volume flow until a failure is triggered. A failure of the oil preheater is clearly distinguishable to the pump and the nozzle, since the pressure drop of the preheater is determinable. A failure of the preheater is caused by a pressure drop, represented by an increase of the pressure loss coefficient ζ_{Pre} in Eq. (10).

Nozzle. Similar to the preheater, the nozzle also suffers filter plugging over the time. The nozzle failure depends mainly on the fuel aging. The failure behavior is modeled according to Eq. (16). The parameters $k_{Noz}/B_K A_F$ depend on the particle loading of the fuel and increase over the time. Under the described conditions, the nozzle has the shortest average failure time.

4.2. Reliability analysis of the system

The system analysis has been performed with 2000 random samples of the validated physical model. The parameters of the Weibull function according to Eq. (1) has been estimated using the least square method. The parameters of the four different simulations with a tank volume of $V_{Tank} = 60$, 40, 30 and 20 l are summarized in Table 3. While the shape parameter β_i is more or less constant for all simulated cases, the characteristic life η_i and the location parameter γ_i decrease with increasing stress level. The constant shape parameter implies that the system fails in the same manner across different stress levels. For completeness, the mean time to failure $T_{MTTF,i}$ of each experimental set i is summarized in the table.

The graphical interpretation of the failure probability is shown in Fig. 10. The abscissa shows the logarithmic difference of the failure time t and the location parameter γ and the ordinate the resulting failure probability. The fit lines for the different tank volumes (and hence stress levels) are depicted as dashed lines. The failure probability is assumed to be a three parameter Weibull distribution, the fit is reasonable for the simulated failure times.

Table 3
Parameters of the reliability analysis for the complete system for various experimental sets i.

i	1	2	3	4	–
V_{Tank}	60	40	30	20	l
s_i	1.00	1.50	2.00	3.00	–
AF_i	1.00	1.17	1.42	1.82	–
η_i	540.80	463.12	379.30	296.98	h
β_i	2.75	2.86	2.61	2.59	-
γ_i	1704.00	1419.44	1271.98	1046.40	h
$T_{MTTF,i}$	2185.31	1832.23	1608.92	1310.10	h

The average failure time decreases with increasing stress factor, since the lines shift to the left side with decreasing volume (increasing stress). Since the shape parameter β_i is constant for all different stress levels, it can be concluded that the tank volume is a suitable stress factor for ALT. The shape parameter is a measure of the variability of the data. Hence, a high shape parameter β_i implies a low variability of the failure time. If the shape parameters differ, other effects would overlap the aging. If different stress levels yield data with very different shape parameters, then either the three-parameter Weibull sampling distribution is the wrong model for the data or we do not have a linear acceleration condition [29].

The impact of the stress factor on failure time is shown in Fig. 11. The figure shows the PDFs for each stress level on a linear time axis. The distribution parameters η and γ and the mean time to failure T_{MTTF} are depicted in the figure. The failure free time γ represents the beginning of the PDF. It is assumed, that no failure occur before this time. The characteristic life of the system is the sum of scale parameter η and location parameter γ. At this time, 63.2% of the systems have failed. The mean time to failure T_{MTTF} represents the time when 50% of the systems have failed. One can see, that each parameter declines with higher stress factor. Since the shape parameter β_i remains constant for all stress factors, the variances of the PDFs decline with increasing stress factor. For a comparison of the experimental failures and the simulated failures, the failure time of the experimental observations have been added in the figure. One can see that the experimental system failures are all within the variance of the numerical analysis.

4.3. Relationship between stress factor and acceleration factor

When using ALT, the transformation to the non-accelerated degradation process is a central issue. Hence, a functional dependency of the stress factor and failure time is desired. A simple approach is a linear transform action of failure time, [33]. The relation between accelerated failure time t_a, non-accelerated failure time t_n and the acceleration factor AF is given by $t_n = AF \cdot t_a$. With Eq. (4) the failure distribution under accelerated conditions can be transformed to non-accelerated conditions. Furthermore, from the parameters of the Weibull distribution in Table 3 the acceleration factor AF can now be estimated as a function of stress factor s. In Eq. (19) the acceleration factor is referred to the failure time at $V_{Tank} = 60$ l and is calculated for each set of experiments. The function type depends on the relationship of lifetime and stress factor (e.g. linear approach, Arrhenius, Eyring, etc.). The acceleration factor can be expressed for each experimental set with

$$AF_i = \eta_1/\eta_i \tag{19}$$

where η_1 is the scale parameter under non-accelerated conditions and η_i the scale parameter for each experimental set. The relation between acceleration factor AF and stress factor s is linear. Hence, the functional relation of the acceleration factor AF can be estimated using a linear fit function with

$$AF = f(s) = 0.4178 \cdot s + 0.5702 \tag{20}$$

as a function of the stress factor s. Based on the experimental data, the relation is assumed to be linear. The numeric values of the linear function have been derived using a least square approach. In the experiments, the volume was decreased from 60 to 20 l. Using the lifetime of the 60 l case as a reference, the equation leads to an acceleration factor of $AF = 1.82$ at $V_{Tank} = 20$ l. This value is in good accordance with the inverse life factor in the experimental analysis of Liška et al. [30]. While the stress factor s is an operating condition, the acceleration factor AF is a statistical parameter that relates a failure distribution of accelerated and non-accelerated life tests.

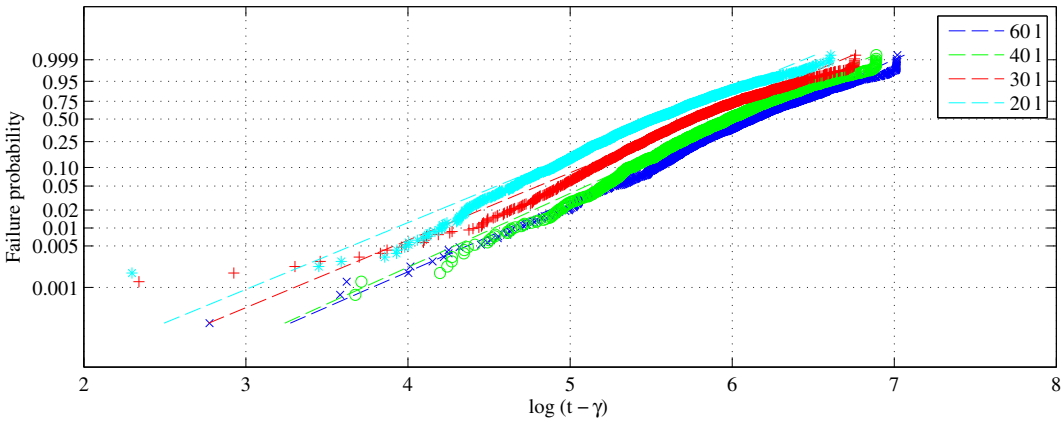

Fig. 10. Failure probability over time and stress factor with $n = 2000$ samples.

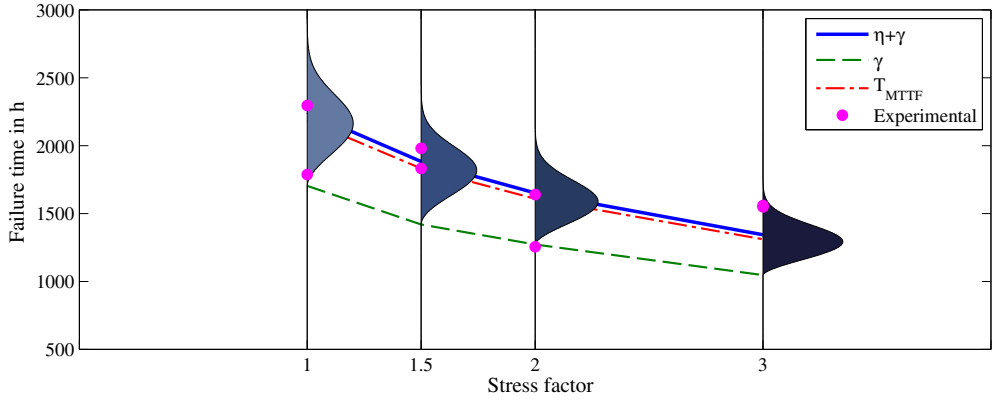

Fig. 11. Distribution of failure time over the stress factor. The experimental failure time data are obtained from Liška et al. [30].

With Eq. (20) a linear relation of operating condition and lifetime acceleration can be concluded.

5. Conclusion

In this paper a simulation approach using physical models for ALT has been presented. The method has been applied on a hydraulic–mechanical part of a fuel supply system of a domestic oil heating system. The test fuel is a blend of 80 vol.% conventional domestic heating oil and 20 vol.% fatty acid methyl ester from rapeseed oil feedstock. The relative residence time $s_i = \tau_1/\tau_i$ could be identified as a suitable stress factor for the ALT. The analysis of the ALT has shown a linear relationship of the stress factor s as a process condition and the acceleration factor AF as a statistical parameter of the test program. Furthermore, the results of the reliability analysis have shown that variances of about 10% of component characteristics lead to a high variance in the failure time of several hundred hours. The variance of the failure time, however, decreases with higher stress factor. For the analyzed experimental set up, a linear dependency of stress factor, acceleration factor and failure probability could be determined.

A major benefit of the presented simulation approach is that the failure analysis of the components is described including the degradation behavior. While the failure analysis describes the relationship of stress factor, acceleration factor and failure distribution, the physical model allows a deep insight of the degradation behavior. The parameters of the physical model are determined by experimental model validation and describe the complete degradation process.

The approach can be used for the description of system failures based on validated numerical models. While the approach is suggested as a complementary analysis of experimental data, the approach can be used for optimization of experimental design as well. With the help of numerical models further applications are possible. The method can be extended on repairable systems in order to optimize the maintenance intervals. Furthermore the model approach can be used to optimize the system reliability. One problem is that such models may become cumbersome. In order to handle with the wide range of time scales, a modeling approach for short term and long term simulations can be combined with the stochastic simulation [34].

Appendix A. Used physical models and statistical data

A.1. Numerical models for the components

The energy balances of an *induction motor* are described with the differential equations for mechanical, electrical and thermal subsystems. A simplified model is introduced with

$$\frac{d\omega_{Mot}}{dt} = \frac{1}{J_{Mot}}[M_{Mot} - M_{Load} - M_{Frict}], \tag{A.1}$$

$$\frac{di_r}{dt} = \frac{1}{L_r}[U_D - k_1\omega_{Mot} - R_r i_r], \tag{A.2}$$

$$\frac{di_s}{dt} = \frac{1}{L_s}[k_2 U_D - R_s i_s], \tag{A.3}$$

Table 4
Summary of the quality data.

Component	Parameter	Distribution	Mean	Standard deviation	Unit
Motor	$C_{Cap,0h}$	Normal	$\mu = 2.99$	$\sigma = 0.0179$	µF
	c_{Cap}	Normal	$\mu = 2.41 \cdot 10^{-4}$	$\sigma = 6.44 \cdot 10^{-5}$	µF h^{-1}
Pump	V_{th}	Normal	$\mu = 2.91 \cdot 10^{-7}$	$\sigma = 4.47 \cdot 10^{-9}$	m^3
	C_{lam}	Normal	$\mu = 1.71 \cdot 10^{-12}$	$\sigma = 2.32 \cdot 10^{-13}$	m^4 s kg^{-1}
	M_c	Normal	$\mu = 0.11$	$\sigma = 0.05$	Nm
Preheater	$\zeta_{Pre,0}$	Normal	$\mu = 0.0013$	$\sigma = 0.00013$	–
Nozzle	β	Normal	$\mu = 10^{-8}$	$\sigma = 10^{-9}$	–

$$\frac{d\theta_{Mot}}{dt} = \frac{1}{mc_{Mot}}[\dot{Q}_{Mot,in} - \dot{Q}_{Mot,out}]. \tag{A.4}$$

The balances contain the mass inertia J_{Mot}, the electrical inertia (inductance) of the stator L_s and the rotor L_r and thermal inertia mc_{Mot} of the motor. The constitutive model equations link the differential equations. With

$$M_{Mot} = mp\frac{(1-\epsilon)\psi}{L_s(1+\epsilon^2\psi^2)}\frac{{U_D}^2}{\omega_s^2}, \tag{A.5}$$

$$M_{Frict} = k_{Frict}\omega_{Mot} \tag{A.6}$$

the equations for the motor torque M_{Mot} and the friction torque M_{Frict} are described [35]. Here, m is the number of phases, p the number of poles, L_s the inductance of the stator, ϵ and ψ are two motor specific parameters. The friction torque is described with the constant k_{Frict} times angle speed of the motor ω_{Mot}. The angle speed of the stator ω_s is proportional to the grid frequency, $\omega_s = 2\pi f_{grid}$. The motor specific parameters are described with

$$\epsilon = 1 - \frac{{L_h}^2}{L_s L_r}, \tag{A.7}$$

$$\psi = \frac{\omega_r L_r}{R_r}, \tag{A.8}$$

where L_h is the main inductance, L_s the inductance of the stator, L_r the inductance of the rotor and R_r the resistance of the rotor [35]. The electrical and thermal balance is coupled with

$$\dot{Q}_{Mot,in} = (R_s + \omega_r(1-\epsilon)L_s\psi/(1+\psi^2))i_s^2 + M_{Frict}\omega_{Mot}, \tag{A.9}$$

$$\dot{Q}_{Mot,out} = \alpha_{Mot}A_{Mot}(\theta_{Mot} - \theta_U), \tag{A.10}$$

where θ_U is the temperature of the environment, θ_{Mot} the motor temperature, α_{Mot} the heat transfer coefficient and A_{Mot} the surface area of the motor.

The capacitor has an important impact on the starting torque of the engine. The capacitor is included with

$$U_D = U_s - R_{Cap}i_s - 1/C_{Cap}\int i_s dt, \tag{A.11}$$

where U_D is the voltage of the motor and $U_s = 230$ V the supply voltage of the grid and R_{Cap} the resistance of the capacitor [36].

The *gear pump* is expressed by static model equations. The mass inertia of the gear pump has an important influence on the acceleration of the induction motor and can be reduced to the motor shaft such that the gear masses are represented in the model. Schlösser [37–40] developed a mathematical model for gear pumps. The volumetric part of the model can be described with

$$\dot{V}_{eff} = \dot{V}_{th} - \dot{V}_{loss}, \tag{A.12}$$

where $\dot{V}_{eff}$ is the effective volume flow, $\dot{V}_{th} = \omega_{Mot}V_{th}$ the theoretical volume flow and $\dot{V}_{loss}$ the volumetric losses. The volumetric losses are divided into a laminar $\dot{V}_{loss,lam}$ and a turbulent $\dot{V}_{loss,tur}$ part, with

$$\dot{V}_{loss} = \dot{V}_{loss,lam} + \dot{V}_{loss,tur} = C_{lam}\Delta p + C_{tur}\Delta p^2. \tag{A.13}$$

Parameter C_{lam} and C_{tur} are loss coefficients for laminar and turbulent losses related to the pressure difference Δp. The constitutive equations for the hydraulic–mechanical part are described with

$$M_{Load} = M_{th} + M_v + M_t + M_p + M_c, \tag{A.14}$$

$$M_{th} = \frac{\Delta p V_{th}}{2\pi}, \tag{A.15}$$

$$M_v = c_{vv}V_{th}\phi_{fl}n_{Mot}, \tag{A.16}$$

$$M_t = c_{tv}\rho_{fl}\frac{n_{Mot}^2}{4\pi}V_{th}, \tag{A.17}$$

$$M_p = c_{pv}\frac{V_{th}\Delta p}{2\pi}. \tag{A.18}$$

The pump torque M_{Load} is the theoretical torque M_{th} plus the torques related to liquid friction M_v, fluid density M_t and pressure difference M_p. Furthermore, V_{th} is the theoretical volume and n_{Mot} the motor speed. The losses are related to dimensionless loss factors for liquid friction c_{vv}, fluid density c_{tv} and pressure c_{pv}.

The *pressure relief valve* can be interpreted as a mass-damper system. The mechanical balance is expressed by

$$m_P\ddot{d} = F_F - F_{p,stat} - F_{p,dyn}, \tag{A.19}$$

with m_K as the mass of the piston, $\ddot{d}$ as the acceleration of the piston, F_F as the force of the helical spring, $F_{p,stat}$ as the static pressure force and $F_{p,dyn}$ as the dynamic pressure force. The force of the helical spring is

$$F_F = c_F(d - d_v) \tag{A.20}$$

as a function of the spring constant c_F and the spring deflection d reduced by the pretension distance d_v. The fluid volume flow acts on the opposite side of the valve. With

$$F_{p,stat} = A_P p_{PRV} \tag{A.21}$$

the static force from the static pressure p_{PRV} and the surface of the piston A_P is described. The dynamic part of the force is described with

$$F_{p,dyn} = \rho_{fl}\frac{\dot{V}_{Pump}}{A_{Byp}}, \text{ with} \tag{A.22}$$

$$A_{Byp} = b_{Byp}(x - d). \tag{A.23}$$

The hole of the bypass A_{Byp} is the product of the hole width b_{Byp}, the position of the valve x and the deflection d. The mass balance of the valve is expressed by

$$\dot{m}_{PRV,out} = \dot{m}_{PRV,in} - \dot{m}_{PRV,Byp}, \tag{A.24}$$

with $\dot{m}_{PRV,in}$ as the ingoing mass flow and $\dot{m}_{PRV,Byp}$ the mass flow of the bypass.

A.2. Temperature and aging behavior of the fuel

The density ρ_{fl} and dynamic viscosity ϕ_{fl} of the fuel are described with the model of Ramírez-Verduzco et al. [41]. The model describes the temperature dependencies and FAME dependency on density and viscosity. The heat capacity of the fuels $c_{p,fl}$ has been modeled using a NASA7 polynomial of a C14H30 reference fuel.

A.3. Quality data of the model parameters

The characteristics of the model parameters are summarized in Table 4. The numerical values of the components induction motor and fuel pump originate from experimental data. For the components preheater and nozzle, the model characteristic has been estimated underlying a typical variance of about ±10% around the nominal value. The values in Table 4 are used for the generation of random numbers.

References

[1] Kvam PH, Bae SJ. Degradation models; 2006.
[2] Cressent R, Idasiak V, Kratz F, David P. Mastering safety and reliability in a model based process. Integrity (RAMS) 2011:1–6. http://dx.doi.org/10.1109/RAMS.2011.5754506.
[3] David P, Idasiak V, Kratz F. Reliability study of complex physical systems using SysML. Reliab Eng Syst Saf 2010;95(4):431–50. http://dx.doi.org/10.1016/j.ress.2009.11.015.
[4] Garro A, Tundis A. A model-based method for system reliability analysis. In: Wainer G, editor. Proceedings of the 2012 symposium on theory of modeling and simulation – DEVS integrative M&S symposium. San Diego, CA: Society for Computer Simulation International; 2012.
[5] Garro A, Groß J, Riestenpatt gen. Richter M, Tundis A. Reliability analysis of an attitude determination and control system (ADCS) through the RAMSAS method. J Comput Sci 2014;5(3):439–49. http://dx.doi.org/10.1016/j.jocs.2013.06.003.
[6] Tinga T. Application of physical failure models to enable usage and load based maintenance. Reliab Eng Syst Saf 2010;95(10):1061–75. http://dx.doi.org/10.1016/j.ress.2010.04.015.
[7] Meeker WQ, Escobar LA. Statistical methods for reliability data. Wiley series in probability and statistics. New York: Wiley; 1998.
[8] Hu C, Zhou Z, Zhang J, Si X. A survey on life prediction of equipment. Chin J Aeronaut 2015;28(1):25–33. http://dx.doi.org/10.1016/j.cja.2014.12.020.
[9] Oh H, Choi S, Kim K, Youn BD, Pecht M. An empirical model to describe performance degradation for warranty abuse detection in portable electronics. Reliab Eng Syst Saf 2015;142:92–9. http://dx.doi.org/10.1016/j.ress.2015.04.019.
[10] Reimer U, Schumacher B, Lehnert W. Accelerated degradation of high-temperature polymer electrolyte fuel cells: discussion and empirical modeling. J Electrochem Soc 2015;162(1):F153–64. http://dx.doi.org/10.1149/2.0961501jes.
[11] Bae SJ, Kim S-J, Park JI, Lee J-H, Cho H, Park J-Y. Lifetime prediction through accelerated degradation testing of membrane electrode assemblies in direct methanol fuel cells. Int J Hydrogen Energy 2010;35(17):9166–76. http://dx.doi.org/10.1016/j.ijhydene.2010.06.045.
[12] McCormick RL, Ratcliff M, Moens L, Lawrence R. Several factors affecting the stability of biodiesel in standard accelerated tests. Fuel Process Technol 2007;88(7):651–7. http://dx.doi.org/10.1016/j.fuproc.2007.01.006.
[13] Mann NR, Schafer RE, Singpurwalla ND. Methods for statistical analysis of reliability and life data. Wiley series in probability and mathematical statistics: applied probability and statistics. New York: John Wiley & Sons Inc; 1974.
[14] Kalbfleisch JD, Prentice RL. The statistical analysis of failure time data. Wiley series in probability and statistics. Hoboken, N.J: J. Wiley; 2002.
[15] D.E. 62506. Methods for product accelerated testing; 2014.
[16] Lu CJ, Meeker WQ. Using degradation measures to estimate a time-to-failure distribution. Technometrics 1993;35(2):161–74.
[17] Lu CJ, Meeker WQ, Escobar LA. A comparison of degradation and failure-time analysis methods for estimating a time-to-failure distribution. Stat Sin 1996;6:531–46.
[18] Meeker WQ, Escobar LA, Lu CJ. Accelerated degradation tests: modeling and analysis. Technometrics 1998;40(2):89–99.
[19] Escobar LA, Meeker WQ. A review of accelerated test models. Stat Sci 2006;21(4):552–77. http://dx.doi.org/10.1214/088342306000000321.
[20] Dowling N. Mechanical behavior of materials; 1993.
[21] Liška M. Untersuchung der brennstoffspezifischen einflüsse auf die betriebssicherheit von ölheizungsanlagen. Ph.D. thesis. Aachen: RWTH; 2009.
[22] Høyland A, Rausand M. System reliability theory: models and statistical methods. Wiley series in probability and statistics, vol. 420. Hoboken: John Wiley & Sons Inc; 2009.
[23] Dunn RO. Antioxidants for improving storage stability of biodiesel. Biofuels Bioprod Biorefin 2008;2(4):304–18. http://dx.doi.org/10.1002/bbb.83.
[24] Tang H, Abunasser N, Clark B, Hirschlieb G, Kim M, Salley S, et al. Quality survey of biodiesel blends sold at retail stations. Fuel 2008;87(13–14):2951–5. http://dx.doi.org/10.1016/j.fuel.2008.04.029.
[25] Pullen J, Saeed K. An overview of biodiesel oxidation stability. Renew Sustain Energy Rev 2012;16(8):5924–50. http://dx.doi.org/10.1016/j.rser.2012.06.024.
[26] Jain S, Sharma MP. Correlation development between the oxidation and thermal stability of biodiesel. Fuel 2012;102:354–8. http://dx.doi.org/10.1016/j.fuel.2012.06.110.
[27] Yaakob Z, Narayanan BN, Padikkaparambil S, Unni S, Akbar M. A review on the oxidation stability of biodiesel. Renew Sust Energy Rev 2014;35:136–53. http://dx.doi.org/10.1016/j.rser.2014.03.055.
[28] Isermann R. Fault-diagnosis systems: an introduction from fault detection to fault tolerance. Berlin: Springer-Verlag Berlin Heidelberg; 2006.
[29] de Souza D, Somani K. Accelerated life testing with an underlying three parameter Weibull model. Engevista 2005;7(1):55–62.
[30] Liška M, Lukito J, van Rheinberg O. Optimierung der prüfmethode für die bestimmung anwendungstechnischer eigenschaften von fame (fatty acid methyl ester) in heizöl el – teil 4: Abschlussbericht für das institut für wirtschaftliche oelheizung e.v. (iwo deutschland) und die erdölvereinigung schweiz; 2008.
[31] Baerns M, Hofmann H, Renken A. Chemische Reaktionstechnik. Lehrbuch der technischen Chemie, 3rd ed., vol. Bd. 1. Weinheim: Wiley-VCH; 1999.
[32] Kulkarni C, Celaya J, Goebel K, Biswas G. Physics based electrolytic capacitor degradation models for prognostic studies under thermal overstress. In: European conference of the prognostics and health management society; 2012.
[33] Dodson B, Nolan D. Reliability engineering handbook. Quality and reliability, vol. 56. New York: Marcel Dekker/Quality Pub.; 1999.
[34] Pohl E, Maximini M, Vom Schloss J, Bauschulte A, Hermanns RT. Degradation modeling of high temperature proton exchange membrane fuel cells using dual time scale simulation. J Power Sources. http://dx.doi.org/10.1016/j.jpowsour.2014.11.054.
[35] Gloor R. Asynchronmaschine; 2013. <http://www.energie.ch/asynchronmaschine>.
[36] Khader S. Modeling and simulation of single phase double capacitors induction motor. In: Proceedings of the 2nd WSEAS international conference on biomedical electronics and biomedical informatics (BEBI '09); 2009. p. 21–7.
[37] Schlösser WMJ. Ein mathematisches modell für verdrängerpumpen und -motoren. Oelhydraulik und Pneumatik 1961;5(4).
[38] Schlösser WMJ, Hilbrands JW. Der volumetrische wirkungsgrad von verdrängerpumpen. Oelhydraulik und Pneumatik 1963;7(12).
[39] Schlösser WMJ, Hilbrands JW. Über den hydraulisch-mechanischen wirkungsgrad von verdrängerpumpen. Oelhydraulik und Pneumatik 1965;9(4).
[40] Schlösser WMJ. Über den gesamtwirkungsgrad von verdrängerpumpen. Oelhydraulik und Pneumatik 1968;12(10).
[41] Ramírez-Verduzco LF, García-Flores BE, Rodríguez-Rodríguez JE, del Rayo Jaramillo-Jacob A. Prediction of the density and viscosity in biodiesel blends at various temperatures. Fuel 2011;90(5):1751–61. http://dx.doi.org/10.1016/j.fuel.2010.12.032.